# Erosion of Retrogressive Thaw Slumps, Herschel Island, YT

by

Jared [William] Simpson

A Thesis Submitted in Partial Fulfillment of the
Requirements for the Degree B.A. in Geography

Department of Geography
McGill University
Montreal (Quebec) Canada

April 2013

## ABSTRACT

Erosion rates of several retrogressive thaw slumps along the Canadian Arctic Coast are studied between 2004 and 2011. Results show a general reduction in the amount of soil eroded as the thaw slumps retreated farther from the coast and presumably stabilized. A 3Dimensional model was created in ArcScene to visualize this decrease in erosion and calculate the volumetric soil loss between each year. Expected soil loss is significant, with over 4000 cubic meters eroding into the Arctic Ocean each year, and creating a very dynamic landscape. The aims of this research are: (1) to create a 3-dimensional model of three retrogressive thaw slumps showing the erosion between 2004 and 2012; and (2) to use the resulting volumetric soil loss values to estimate soil organic carbon (SOC) flux into the Arctic Ocean. Results show a substantial amount of soil loss totaling over 160,000m3 and a subsequent SOC flux of over 13 million kg. These findings suggest that retrogressive thaw slumps have significant environmental impacts and that further research is needed to better understand these dynamic landforms.

## ACKNOWLEDGEMENTS

This honours thesis would not have been completed without the help of some incredible people. First and foremost is of course Professor Wayne Pollard, who introduced me and gave me the opportunity to pursue Arctic research. Wayne has impacted my life more than anyone else (with the exception of my parents). He is an amazing supervisor, the best boss I have ever had, and an incredibly generous human being. I would never have had the confidence to walk up and talk to an extremely accomplished professor however without the influence and everlasting support of my loving family. My Dad instilled in me an incredible work ethic (any job worth doing is worth doing right) and my Mom a seemingly endless supply of optimism, while my brother has taught me to always keep striving with his uncanny ability to be better than me at everything.

A lot of work has been put into this thesis, both in the field and in the office. I would therefore like to thank all of those who put in their time to help me along the way: Professor Bernhard Lehner for being my reader and sending me very helpful comments even when on sabbatical; Dave Fox for all his encouragement in the field; Mike Angelopoulus for his help editing and making 16 hour days in the field a delight with his wacky sense of humour; Heather Cray-Sloan for her endless advice and willingness to help with almost any problem; Joseph Ariwi for being my go-to designer; Natalie Cornish for her endless compliments, support, and uncanny ability to make me smile; and Courtney Claessens for her help with my references. I owe all of you more than I could ever repay.

## Contents

# List of Figures

# List of Tables

# CHAPTER 1 - INTRODUCTION

Over the past few decades the coast of the Western Canadian Arctic has been the focus of several studies concerned with the effects of global warming on coastal systems (Hoque & Pollard 2009; Lantuit & Pollard 2003, 2005). Since these coasts are in the continuous permafrost zone and many are ice-rich, even a small change in temperature can have a dramatic effect on the depth of the active layer, thermokarst and coastal erosion.

Retrogressive thaw slumps, a common thermokarst landform, have been increasing in both frequency and extent, particularly along exposed coasts (Lantuit & Pollard, 2005). Warming temperatures, changing sea ice and open water conditions, and changing wave climate are considered one of the main causes of increased coastal erosion and related thermokarst activity (Forbes et al., 2011). Together with coastal erosion and thermokarst is the potential increase in soil organic carbon (SOC) flux into the Beaufort Sea. The impact of SOC flux is potentially far reaching.

Unique among the world's oceans the Arctic Ocean is surrounded by land, with only a few transport corridors for nutrient exchange between oceans such as the Fram Strait. The Carbon cycle of the Arctic Ocean is therefore influenced greatly by riverine and coastal sources of organic carbon (Figure 1.1) (Stein & Macdonald, 2004). The influx of carbon from rivers is disproportionate when compared to the other large oceans, the Arctic Ocean containing only 1 percent of the world's ocean volume and receiving 10 percent of the global terrigenous dissolved organic carbon

(DOC) load (Opsahl et al., 1999). The contribution of carbon into the Arctic Ocean from coasts is generally proportionate to that of riverine systems (Stein & Macdonald, 2004). As Arctic coastlines become increasingly sensitive to climate change an increase in coastal erosion and subsequent carbon flux into the ocean will occur. For this study, SOC is of particular interest, as the study region has been shown to be a significant input (Couture, 2010). There is an immediate need for more detailed analysis of Arctic coastal erosion and its impact on both geomorphology and biogeochemical systems.

This study focuses on the nature and rate of thermokarst for an area of ice-

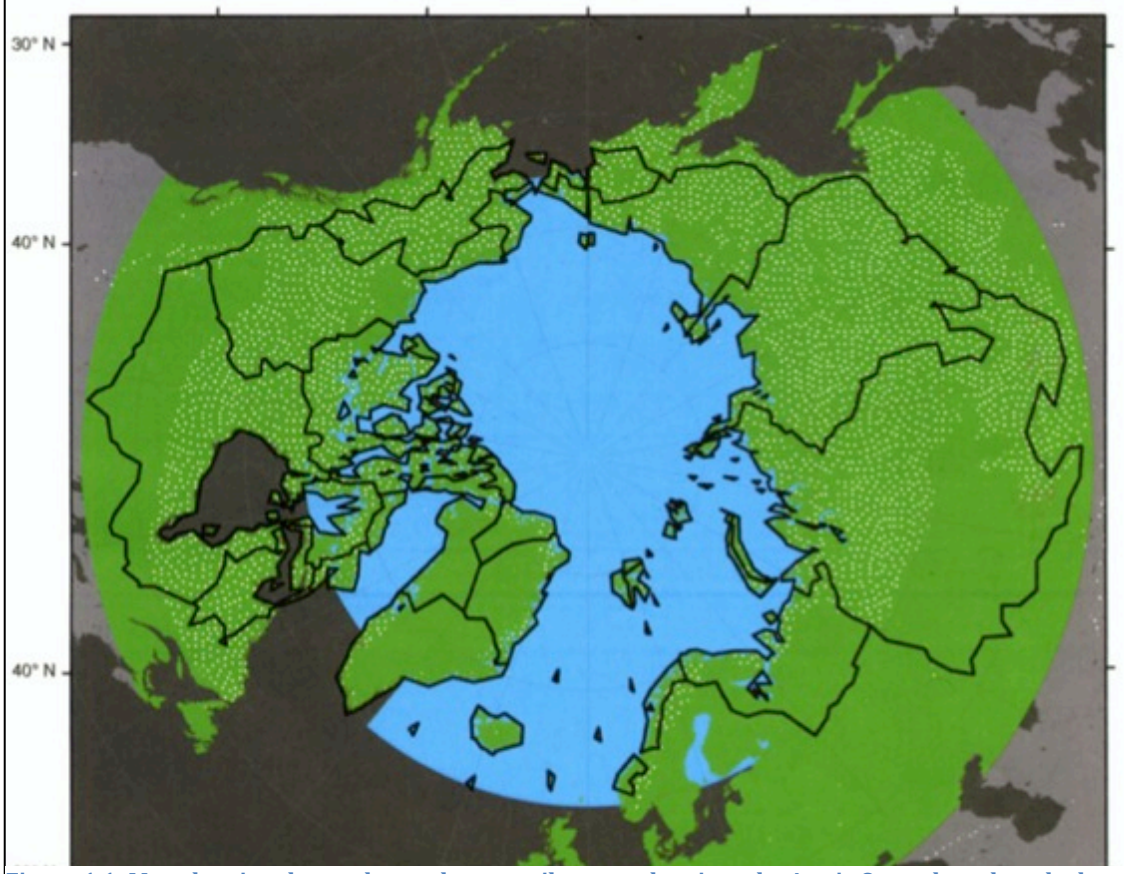


**Figure 1.1: Map showing the total area that contributes carbon into the Arctic Ocean based on the large scale circulation of the Arctic Ocean, hydrology, and the land areas underlain by permafrost. The heavy black outlines denote large-scale watersheds that drain into the Arctic Ocean, while the white striped areas is unglaciated land underlain by permafrost. Leif Anderson created the area designation, watershed boundaries are derived from Lammers et al. (2001), and the permafrost distribution is based on maps from the National Snow and Ice Data Center (Brown et al., 1998).**

rich permafrost. My hypothesis is that current levels of coastal thermokarst are a potential source of soil organic carbon for Arctic Ocean systems, and the use of GIS-based analysis is an effective method of assessing both geomorphic and biogeochemical fluxes. The aims of this research include: (1) creating a 3-dimensional model of three retrogressive thaw slumps showing the erosion between 2004 and 2012; (2) using these models to estimate erosion volumes and (3) using the resulting volumetric soil loss values to estimate SOC flux into the Arctic Ocean.

The main study site is located on Thetis Bay along the southeast coast of Herschel Island, Yukon Territory (Figure 1.2).

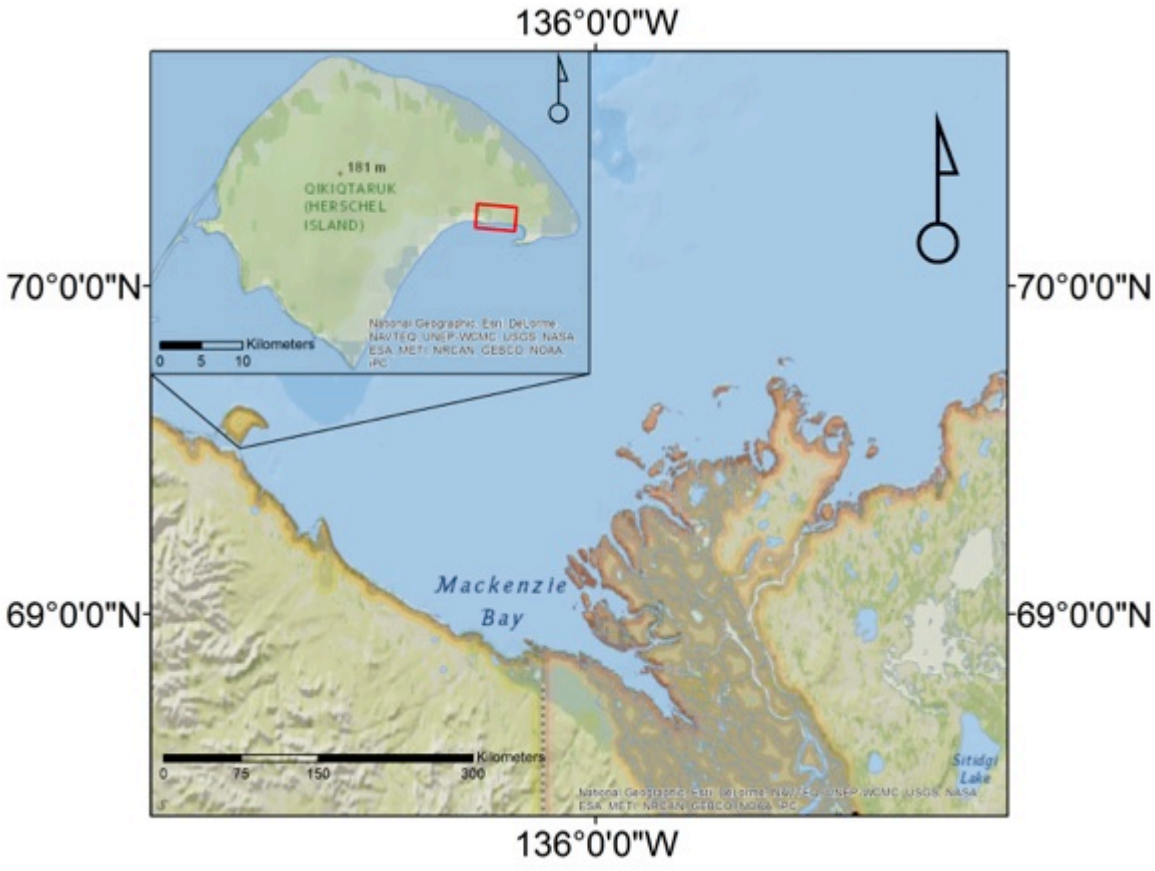


**Figure 1.2: Location of Herschel Island, YT. The red box indicates the location of the study site. Source: National Geographic, ESRI basemap.**

Three retrogressive thaw slumps (A, B, and C) were chosen as a representative sample for this case study due to their differing sizes (Figure 1.3). The continuous permafrost of Herschel Island is known to be extremely ice-rich (Fritz et al., 2011), making it vulnerable to thaw-related processes like thermokarst. Liquefied soil created by the rapidly retreating thaw slump flows into the ocean carrying with it a range of materials (SOC, mercury, methane, etc). In order to better understand the dynamic nature of these thermokarst landforms Differential Geographic Positioning System (DGPS) points taken annually between 2004 and 2012 were used to create a 3-Dimensional representation of volumetric soil loss within ESRI's ArcScene program. A landscape surface from thousands of years ago was also modeled in order to better understand the geomorphology of the land, and to estimate volumetric sediment loss.


**Figure 1.3: Retrogressive thaws slumps A, B, and C on Herschel Island, YT. Photo source: JSimpson Photography**

In chapter 2 a review of the background literature will be presented in order to understand the importance of this long-term case study. Chapter 3 will detail the data and methods used throughout this thesis, while chapter 4 will explain the results and look at any trends or anomalies found. Chapter 5 offers an analysis of the data and details their importance, as well as any sources of error within the study. Finally, chapter 6 concludes with the main findings of this thesis and their contribution towards the larger body of literature.

# CHAPTER 2 – BACKGROUND LITERATURE

## 2.1 – Permafrost

Permafrost is defined as ground (e.g. soil or rock) that has stayed below 0°C for more than two years (French, 2007). Moisture such as water or ice may or may not be present however. Although defined in thermal terms it is useful to characterize permafrost by both its temperature and state. The terms 'cryotic' (material below 0°C) and 'non-cryotic' (material above 0°C) are therefore useful when characterizing permafrost, as they describe only the thermal condition of the soil. A typical ground thermal regime for permafrost soils is shown in Figure 2.1.

Several other terms are used to help describe the thermal structure of permafrost. The permafrost table is the upper limit of cryotic conditions, and the ground directly above the permafrost table is called the supra-permafrost layer and includes the active layer. The active layer is ground which thaws and freezes each year, the depth of which is determined in large part by summer air temperatures and soil characteristics (French, 2007). The active layer depth is positively correlated with the summer surface temperature. For example, an increase in mean surface temperature will cause an increase in active layer depth, while a decrease in surface temperature will cause the opposite during the months below 0°C. Unfrozen zones can exist between the bottoms of the seasonal frost zone and the permafrost table, as well as within the permafrost table itself. These unfrozen zones are called taliks.

Permafrost occurs in two distinct yet sometimes overlapping areas, high altitudes and high latitudes. It can therefore be classified into three different categories, (1) polar permafrost, (2) alpine permafrost, and (3) plateau permafrost such as that found in the Gobi desert (French, 2007). Approximately 23-25% of the northern hemisphere is underlain by permafrost, emphasizing the extent of this dynamic geomorphology. The distribution of permafrost differs mainly according to climate, and is classified according to its distribution as continuous (90-100%), discontinuous (50-90%), sporadic (10-50%) and isolated (0-10%) as seen in Figure 2.2. In North America the distribution of cryotic soils is governed by climate, with the southern reaches of permafrost corresponding with the -1°C mean annual air temperature isotherm (Brown, 1960; Péwé, 1966).

| | Area, $10^6$ km$^2$ (%) | | | | | |
|---|---|---|---|---|---|---|
| Extent of permafrost | Lowlands/uplands with thick overburden | | | Mountains with thin overburden | | |
| | High >20% | Med 10–20% | Low 0–10% | High >10% | Low 10% | Total |
| Continuous (90–100%) | 1.49 (5.9) | 1.31 (5.1) | 0.38 (1.5) | 2.14 (8.4) | 5.66 (22.2) | 10.98 (43.1) |
| Discontinuous (50–90%) | 0.08 (0.3) | 0.87 (3.4) | 0.38 (1.5) | 0.75 (2.9) | 2.34 (9.2) | 4.42 (17.3) |
| Sporadic (10–50%) | 0.11 (0.4) | 0.31 (1.2) | 0.56 (2.2) | 0.32 (1.3) | 2.66 (10.4) | 3.96 (15.5) |
| Isolated (0–10%) | 0.34 (1.3) | 0.07 (0.3) | 0.60 (2.4) | 0.03 (0.1) | 2.85 (11.2) | 3.89 (15.3) |
| Relict | | | | | | 0.12 (0.5) |
| Total area | 2.02 | 2.56 | 1.92 | 3.24 | 13.51 | 23.37 |
| Permafrost (%) | (8.6) | (11.0) | (8.3) | (14.1) | (58.2) | (100) |

**Figure 2.1: The extent and ice content of permafrost (*Frozen Ground*, 22, 1998)**

The many problems related to permafrost soils are related to the water or ice content, which determines various physical characteristics of the soils. Three main categories of problems are described in French (2007), and include: (1) ice segregation, (2) the different hydrologic characteristics of cryotic soils compared to non-cryotic soils, and (3) ground ice thaw.

The freezing of water within the soils results in ice segregation, which can cause ice heave and cracking similar to that which is found in desiccated mud (French, 2007). The amount of displacement is directly related to the available moisture. The more moisture there is more water to freeze and expand, pushing outwards on the surrounding soil. Ground ice thaw is another significant problem as large amounts of ground ice can be found within permafrost soils (Couture, 2010).

## 2.2 - Ground Ice

The term 'ground ice' is used to refer to any ice which forms in freezing or frozen rock, and can occur in pores, cavities, voids, or any space between soil and rock (ACGR, 1988). Unconsolidated soils can be especially ice rich, with the amount of ice exceeding saturation – the volume greater than saturation referred to as excess ice. Massive ice refers to more-or-less continuous bodies of nearly pure ice or ice-rich sediment with considerable excess ice. The thawing of excess ground ice can cause significant ground subsidence. Related is that soils cemented together with ice have significantly different physical (rheologial) properties than unfrozen soils (Tsytovich, 1973). Fine grained soils are especially at risk as the thaw of pore

and segregated ice can cause liquefaction and a drastic decrease in bearing strength, leading to erosion (French, 2007). For the purposes of this study, only ground ice within unconsolidated materials is considered.

There are two main metrics used when discussing ground ice within unconsolidated materials, ice content and the amount of excess ice. Ice content is the amount of ice within a sample and can be expressed either gravimentrically or volumentrically (French, 2007). For example, if a sample was found to be 100g when frozen and 40g when oven dried, the gravimentric ice content would be 60g which is 60% total weight, or 150% on a dry weight basis. Soils are classified on their ice content. Low ice content soils have values between 40-50%, and high ice-content soils between 50-150% (French, 2007). In general, the finer grained the material, the more void space and thus the higher ice content it can have. This is particularly true of silts; however the pore size in clay is so fine that it limits soil water processes. Excess ice is the second important ice content variable, and is calculated as the volume of water in excess of saturation - referred to as supernatant water (French, 2007). For example, when a sample is taken and allowed to thaw, the amount of saturated sediment and excess water can be measured. The resultant supernatant water is expressed as a percentage of the total volume of the sample. This measurement is useful as it gives an indication of the amount of ground subsidence that might occur if frozen sediment were to thaw. There are also large ice bodies called 'massive ice' that have an ice content measurement of at least 250%.

A common genetic ground ice classification system used today is based on the source of water immediately prior to freezing and the main process which transports water to the plane at which freezing occurs (Figure 2.3) (Johnston, 1981; Mackay, 1972). The system emphasizes the many different mechanisms of water transport such as sublimation, gravity transfer, soil- water expulsion, and the effects of soil-water pressure and the soil-water gradient. It focuses on four main ground ice types, (1) wedge ice, (2) segregated ice, (3) intrusive ice, and (4) pore ice.

Pore ice or interstitial ice cements soil grains together. It occurs when water infiltrates into the sediment and is frozen in-situ, bonding the grains and filling the

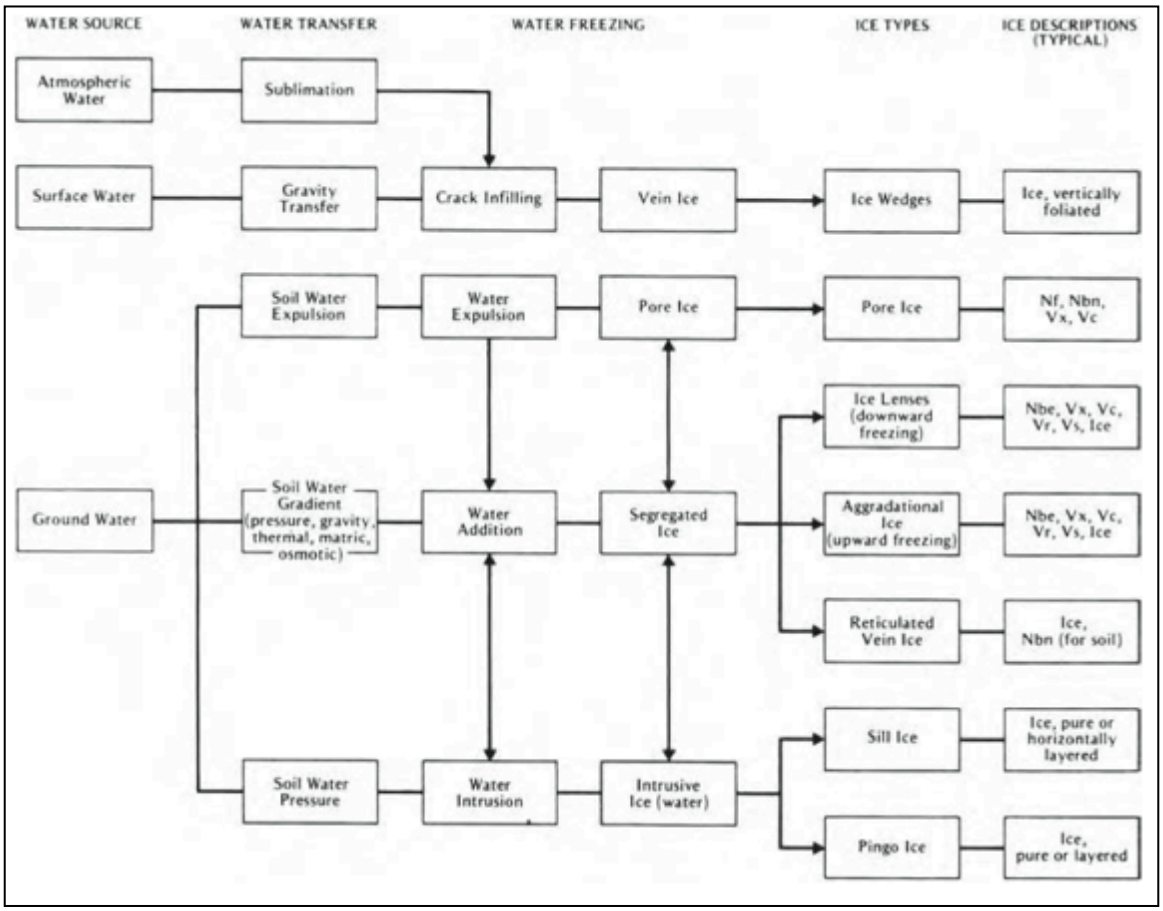


**Figure 2.2: Classification of ground ice based on the water source and the main transfer process at the time of freezing (Modified from Mackay, 1972), with ice descriptions from Pihlainen and Johnston (1963).**

void spaces. Intrusive ice forms when water intrudes under pressure into the seasonally frozen zone (French, 2007). Segregated ice is a general term for soil with high ice content. It can form in many different materials; however fine-grained sediments are especially suitable because of their high porosity (French, 2007). Wedge ice occurs when water penetrates into cracks or fissures in the sediment, and commonly creates ice wedges, which will be discussed in the Thermokarst section.

The volume of ground ice within permafrost varies depending on the host material. Table 2.1 illustrates the difference between the ice content in the bedrock of the Fosheim Peninsula, Ellesmere Island, opposed to the ice content in the unconsolidated sediment of the Western Canadian Arctic.

## 2.3 - Thermokarst Activity

Thermokarst is the process by which local or widespread erosion, collapse, ground subsidence, and instability of the ground surface occurs through the thawing of permafrost and a deepening of the active layer (French, 2007). The varying reasons for an increase in the active layer are outlined in Figure 2.4. Origins of permafrost degradation are classified as climatic, geomorphic, or vegetational, and whether or not they were induced through anthropogenic forces.

**Table 2.1: Ice contents in percentage for different areas (Harry et al., 1985; Pollard & French, 1980; French & Harry, 1983; Couture & Pollard, 1998).**

| A. Upper 5.0m of permafrost, unconsolidated sediments, Western Arctic | | | |
|---|---|---|---|
| | Pore/Segregated ice (%) | Wedge Ice (%) | Total ice (%) |
| King Point, Yukon | 43 (79) | 11 (21) | 44 (100) |
| Richards Island, NWT | 28 (79) | 7 (21) | 36 (100) |
| Southwest Banks Island, NWT | 44 (77) | 21 (37) | 56 (100) |

Predicting where thermokarst activity will occur is problematic due to the variability of climate, permafrost, and ground ice across the globe. However, some generalizations are appropriate however. First, thermokarst occurs mostly in unconsolidated and ice rich materials, reflecting the physical properties of the soil (French, 2007). The large pore spaces between the fine-grained sediments aid ice segregation and heat transfer. Second, is that thermokarst is rarely reported from alpine permafrost regions due to the majority of the material being bedrock (French, 2007). Finally, thermokarst rarely occurs in the ice-free regions of the poles (French, 2007).

The two main results of thermokarst are erosion and subsidence; however the processes by which the two happen are different. Subsidence occurs when

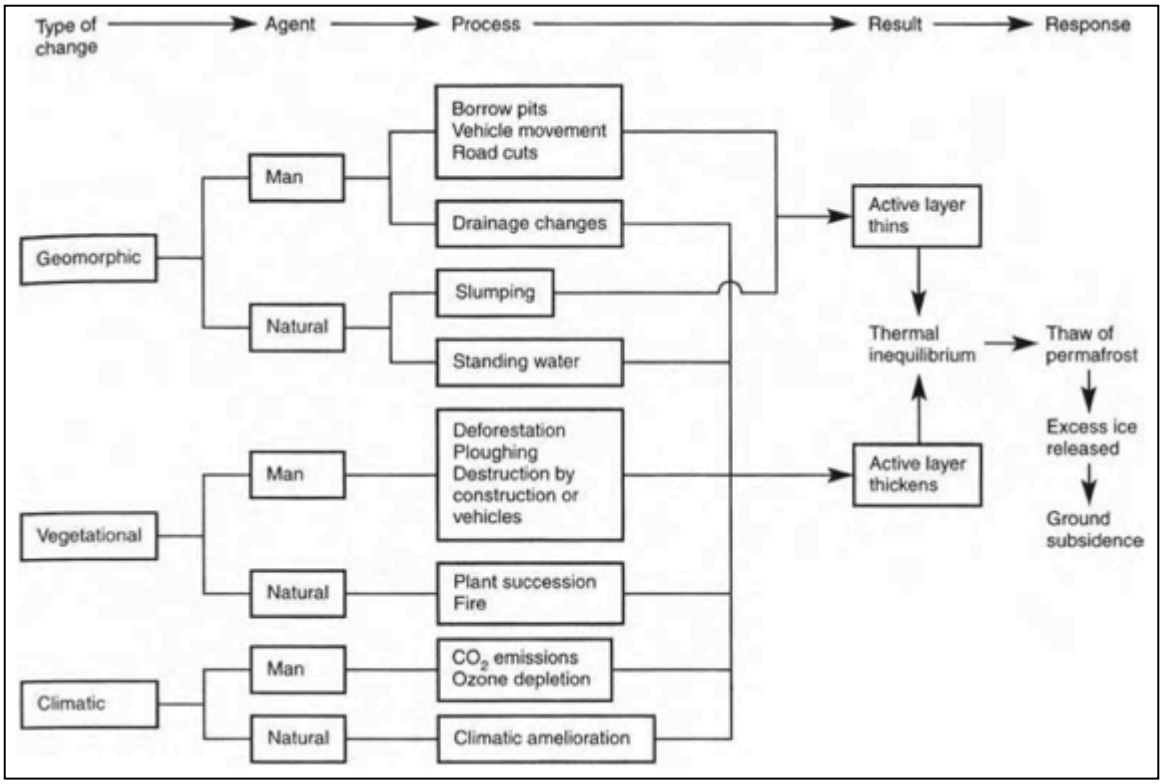


**Figure 2.3: Diagram of how different forces cause permafrost degradation. In this study the climatic forces are most important variables (French, 2007).**

excess ice thaws and the resulting excess water evaporates or is drained (French, 2007). Thermal erosion occurs through a series of erosional processes linked with running water, which act upon ice-rich permafrost (Romanovskii, 1961; Shamanova, 1971). It occurs when flowing water from sources (i.e. run-off, snowmelt, or thaw) are concentrated along ice wedges and cause more preferential thaw (e.g. tundra ponds) (French, 2007). This in turn creates more flowing water that erodes the surrounding materials. Erosion can be significant. Landforms such as retrogressive thaw slumps are one of the most rapidly erosive processes in periglacial environments today (French, 2007). Retrogressive thaw slumps are widespread, and are concentrated along the coast because of the added erosional forces of waves.

Retrogressive thaw slumps are a type of backwasting thermokarst activity that is common along the coasts of the Arctic Ocean in areas of massive ice bodies (Figure 2.5). Generally these landforms are caused by wave activity along the coast and subsequent thaw in areas of active coastal retreat. When the ice within these C-shaped depressions starts to thaw, the surrounding soil is liquefied and begins to erode away from the vertical face, and back wasting occurs (Lantuit et al., 2005). They can reach lengths of up to 650m, widths of more than a kilometer, and vertical heights upwards of 10m (Lantuit et al., 2012). The Southern Beaufort Sea region is one of the most ice rich areas in the Canadian Arctic, and has many retrogressive thaw slumps both inland and along the coast (Pollard, 1990; Pollard and French, 1980). The permafrost soils that underlie the entire area are rich sources of soil organic carbon (SOC) and greenhouse gases (Bockheim et al., 1999; Oechel et al.,

1995). If the amount of SOC within the permafrost soils is known, than the volume of sediment erosion can be used to estimate the potential volume of SOC flux into the Arctic Ocean from the coastlines (Rachold et al., 2003). There is a potential that an increase of this influx could have an effect on the carbon balance of the Arctic Ocean, causing widespread changes (Rachold et al., 2003). Most climate change scenarios show an increase of erosion correlating with an increase in temperature, however as there are very few long-term studies of volume loss due to thaw (Lantuit et al., 2005) or carbon content (Couture et al., 2008), the potential contribution of retrogressive thaw slumps is unknown (Lewkowicz, 1991).

The variable nature of ground ice continues to hinder prediction and analysis of thaw slumps (Pollard & French, 1980), and their remote setting makes direct

**Figure 2.4: Large retrogressive thaw slump with entrained ice bodies on Herschel Island, YT. As the ice melts it liquefies the surrounding sediment and decreases its sheer strength, resulting in massive erosion. Source: JSimpson Photography**

observations difficult. Recent studies (Lantuit et al., 2005) have employed remote sensing techniques to quantify the amount of erosion during thaw slump occurrence with mixed results; however no study has used a combination of remote sensing and more traditional surveying methods to analyze erosion rates and volumetric loss. The potentially significant impact of these retrogressive thaw slumps on the Arctic carbon cycle makes them an interesting object of study, and an accurate three-dimensional model of the erosion over many years would be a valuable asset for future climate change impact models.

## 2.4 - The Arctic Coast

The presence of sea ice governs many different coastal processes in the Arctic, especially the geomorphology and stability of unconsolidated shorelines. A thin cover of ice over the surface of the ocean acts as a buffer against the propagation of wind driven waves, and mitigates surface wave generation (Squire, 2007). Perennial sea ice has greatly reduced the fetch of waves, and thus reduced the destructive influence they have along the Arctic shorelines. With the probability of the sea-ice disappearing over the summer months however, both of these mitigating factors could disappear and the Arctic coasts could erode at an alarming rate.

Storms can cause heavy erosion along coastlines due to the large waves and surges brought by heavy winds. Wave action is the primary source of erosion along the Arctic coastlines, which along with temperature and precipitation plays a

significant role in determining the coast's geomorphology. Recent studies (Ogorodov, 2008) have shown that there is an inverse relationship between ground-ice content and wave action In general however, the limited wave action due to the presence of sea-ice, means that wind-induced waves predominate. The reduction in sea-ice extent will increase the amount of fetch available and cause larger and more powerful swells. The definite trend of rising temperatures and reduction of sea ice extent is significantly altering the Arctic coastline, and the projected increase in these environmental changes will continue as temperatures rise (Forbes et al., 2011).

Up to 65% of the Arctic coastline is made up of unconsolidated, ice-bonded material (Lantuit et al., 2011). The presence of the ice lends the sediments intrinsic strength; however it also means that thawing could create widespread erosion. Combinations of geologic and biologic properties of coastal materials (e.g. ice content, vegetation, and sediment type), the coastal morphology (e.g. exposure, elevation, and slope), and the way in which the coastlines control the interaction between the climate and oceanographic forcing (e.g. waves, sea and air temperature) are all factors which influence the highly varied erosion rates along the coastlines of the Arctic (Forbes et al., 2011)

Only averages of multiple events can be accurately measured and studied due to the logistical difficulties in Arctic research (Lantuit et al., 2011). Discerning the impacts that climate change has had on the Arctic Coast is difficult and the subject controversial. Solomon (2005) reports no statistically significant changes in decadal patterns since the 1970's, while Vasiliev et al (2005) describes a cyclic

pattern, which could be due to the regional or global weather oscillation events. Recent papers have measured rapid and significant increases in erosion rates however (Brown et al., 2003; Mars and Houseknecht, 2007; Arp et al., 2010; Jones et al., 2009), and evidence suggests that the increase is caused by the retreating sea ice, an increase in sea surface temperature (Jones et al., 2009; Overeem et al., 2010; Barnhart et al., 2010) and the subsequent increase in the severity and frequency of storm events (Brown et al., 2003; Arp et al., 2010).

Increased coastal erosion has had accumulative environmental and ecological effects. Many ecosystems depend on long beaches along unlithified coasts for breeding and nesting sites (e.g. eider ducks), and many anthropogenic communities also occupy this space. Industrial infrastructure has also been threatened. Along with many buildings, sewage and landfill facilities occupy land that has come under increased risk of erosion. If these facilities were to collapse they could cause damage to both the environmental and human health.

# CHAPTER 3 - METHODOLOGY

## 3.1 - Research Design

This study represents experimental research into the quanitfication of retrogressive thaw slumps. A small case study of three retrogressive thaw slumps is attempted using GIS and Remote Sensing technologies to quantify the amount of erosion that occurred between 2004 and 2012.

My conceptual framework mainly encompasses methodological queries and which technology is best suited to both the remote environment I worked in and the consequential logistical difficulties. The identification of the surrounding terrain and the main geomorphological factors contributing to the thermokarst activity are also sources of valuable knowledge about retrogressive thaw slump behaviour.

## 3.2 - Data Description

The spatial data layers used in this study are in the projected coordinate system WGS_1984_UTM_Zone_7N and the H2L geoid datum.

### *3.2.1 - Elevation*

The Hershel_2m_DEM Digital Elevation Model (DEM) was extracted from a 2000 IKONOS panchromatic stereo-pair using the method described by Toutin et al. (2001). This 2001 DEM covers Herschel Island and has a 2m horizontal resolution and a 2cm vertical resolution (Lantuit & Pollard, 2005). Field data collected by

Hugues Lantuit in the summer of the same year using the Kinematic Differential Global Positioning System was used to validate the DEM.

### *3.2.2 - DGPS points*

Twenty-four shapefiles contain DGPS points recorded by Hugues Lantuit (2004-2006), Heather Cray-Sloan (2007-2010) and Jared Simpson (2011 and 2012) of McGill University around the perimeter of retrogressive thaw slumps A, B, and C. These data were collected yearly between 2004 and 2012 using a Trimble 5700 Differential Global Positioning System (DGPS). The shapefiles were then post-processed using Post Processed Kinematics (PPK). The DGPS points have elevations in meters above sea level with a sub-5cm vertical and horizontal accuracy (Trimble, 2005)

## 3.3 - Data Collection

### *3.3.1 - Headwall Outlines*

During the summer months, when data collection is possible, the slumps are very active and large clumps of material fall from the edge without warning. As some of the headwalls are over 5m in height, with sheer sides that lead into mud pools that can be over 3m deep, great care must be taken when collecting data. Due to these safety issues, the DGPS points were taken approximately 0.5m away from the edge of the headwall. During the 2006 field season however, slump C was deemed too dangerous for data collection to occur around its headwall. To correct for this error, the time spans were divided into one-year increments with an

estimated linear regression rate. A point was taken approximately every 5m along the headwall. I then input the points into a GIS for further analysis.

### *3.3.2 - Digital Elevation Models*

I created a digital elevation model of each slump floor using DGPS points and interpolation. Over 500 points for each slump were taken by me over the 2012 field season (Figure 3.1).

In order to obtain the most accurate interpolated result, data points were taken along transects and as a result of decisions made in-situ depending on the local topography. This ensured that any ridges or mounds that would not have been

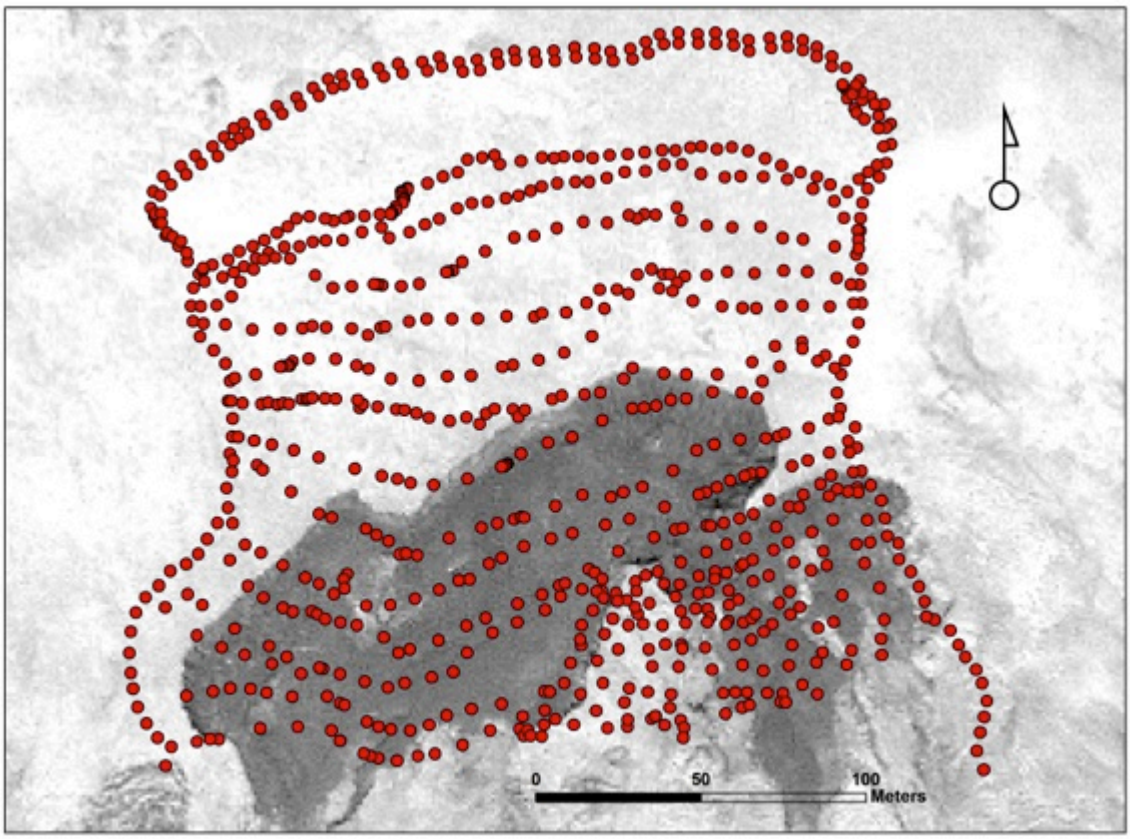


**Figure 3.1: DGPS points used for interpolation of the slump floor DEM. Points were taken in approximately linear transects with more points taken around important features (e.g. streambeds, abrupt elevation changes, etc.).**

properly represented by the linear transects were shown. Due to site conditions (e.g. mud pools) points could not be taken near the slump headwall. The positions and elevations of the points were therefore estimated using measuring tapes with an accuracy of 5 cm. After several trial and error tests of different interpolation methods such as IDW and splining, the krige interpolation method was found to create the most visually accurate DEM's.

### *3.3.3 - Soil Organic Carbon and Ice Content Measurements*

Organic carbon and ice content measurements were taken from previous research (Couture et al., 2010) and verified with samples from the field during the July 2012 field season. A sample from a massive ice body, reticulated ice, and the active layer were taken from the headwall of each slump and brought back to the lab for analysis. The samples were weighed, then put into an oven to dry and weighed again to determine volumetric ice content using the following equation:

$$W = Wi + Wu$$

Where $Wi$ is the ice content and $Wu$ is the unfrozen water content. The dry samples were then baked in an oven at 800°C to burn off any organic matter and weighed again to determine soil organic content. The resulting measurements were consistent with previous studies at approximately 86kg/m$^3$

## 3.4 - Data Analysis

### *3.4.1 - Post-Processed Kinematic Positioning*

Post-Processed Kinematic (PPK) surveying was used to take GPS measurements in the field over a wide area and a short time span (Figure 3.2). A continuous kinematic surveying technique was employed because it is useful for taking many measurements over large areas when there is little obstruction to satellites. A base station recorded the positions of every satellite each second for the entire study period was placed over a known benchmark on Herschel Island. I then took a rover receiver into the field and recorded GPS points of areas of interest, with the relative location of the rover measured at each epoch (Figure 3.2). This

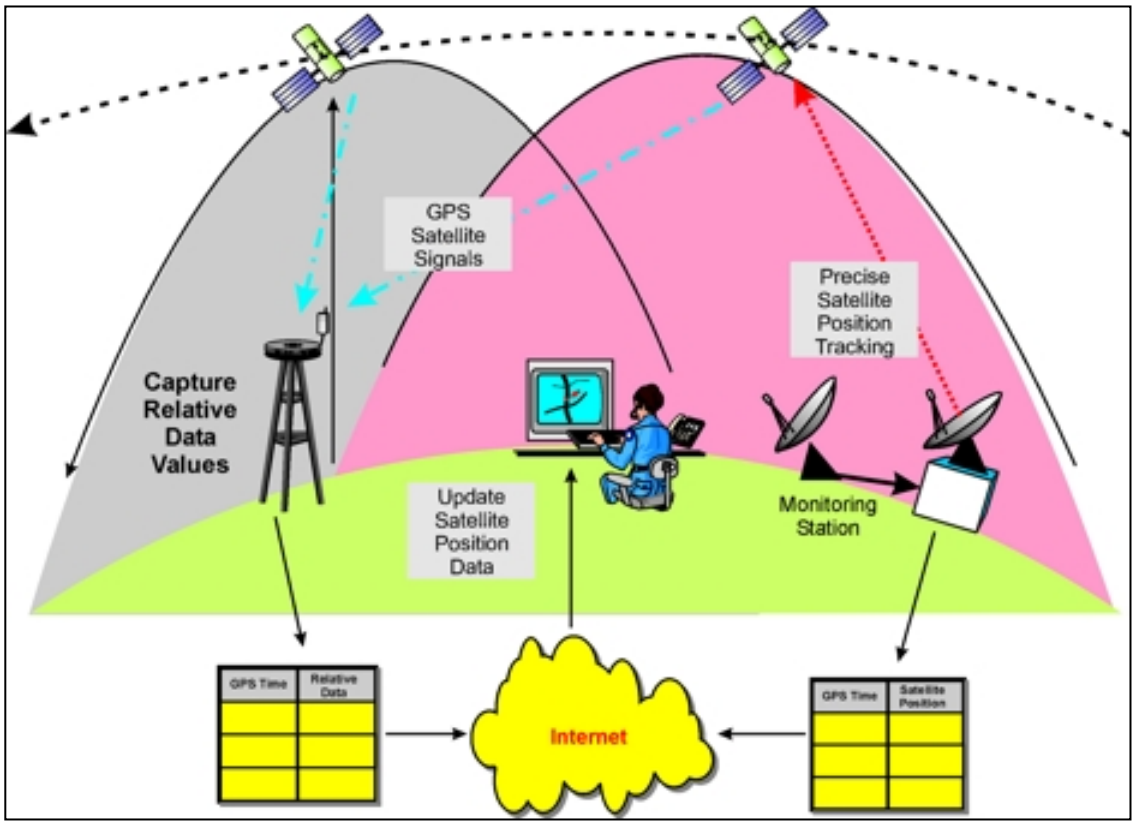


**Figure 3.2: Diagram of Post-Processed Kinematic (PPK) correction of dGPS points (Wirelessdictionary.com). The base station takes measurements of the positioning of the satellites each second, and then uses this information to correct the positioning of dGPS points taken in the field**

information was then combined to retrieve corrected data with a vertical and horizontal accuracy below 5cm (Trimble, 2005)

### *3.4.2 - Volumetric Loss*

To determine the volumetric loss between each year, the area between each year's headwall was calculated using ESRI's ArcMap program. A polygon was created by connecting the spot heights of each slump headwall between $year_x$ and $year_{x-1}$ to determine the area of loss for each successive year (Figure 3.3) (Appendix A.1).

The 2001 DEM was then corrected using the slump floor DEM's created via krige interpolation (Appendix A.2). The result was the volume between the DEM of

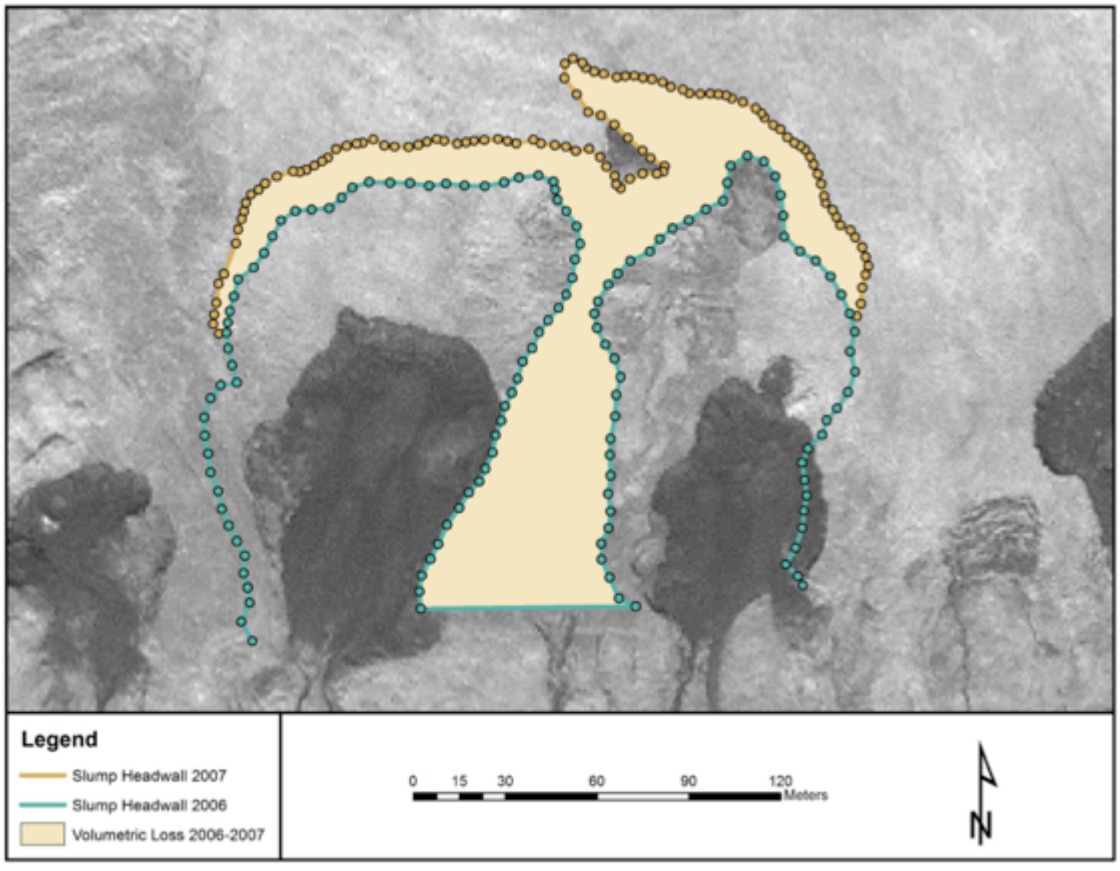


**Figure 3.3: Example of the polygons used to extract the portion of the DEM used to calculate volumetric loss. The dGPS points were used as markers for where the headwall was each year, and the polygons created to measure between years. This process was repeated each year for each slump.**

the surface in 2001 and the DEM of the slump floor in 2012. The created polygons were used as outlines to clip the DEM producing raster data files for each year (Appendix A.3). Volumetric loss for each raster was calculated using a simple subtraction and soil –ice ratios and soil organic carbon values for the study area were obtained from Couture (2010) and used to calculate a resulting volumetric soil loss and SOC flux. Patterns and trends found were graphed in Microsoft Excel for a visual representation of the analysis (Appendix A.4).

A 3-dimensional model was also created in ArcScene to give a visual representation.

### *3.4.3 - Percent Area Loss*

Percent area loss was calculated in order to observe the amount of erosion undergone within each slump compared to its respective area. The values were calculated by dividing the amount of area lost each year by the total amount of area lost over the entire study period. The total percent lost for each slump is below 100% as the slumps were already established before the first year of data collection.

### *3.4.4 - Original Surface Reconstruction*

An estimation of what the surface of Herschel Island's coastline would have been like before slump activity was created using DGPS points and krige interpolation methods (Figure 3.4). The DGPS points were taken along the ridge above the three study slumps and along the coast to estimate the surface's slope. Krige interpolation methods were applied to the DGPS points, and an estimated surface reconstruction was created.

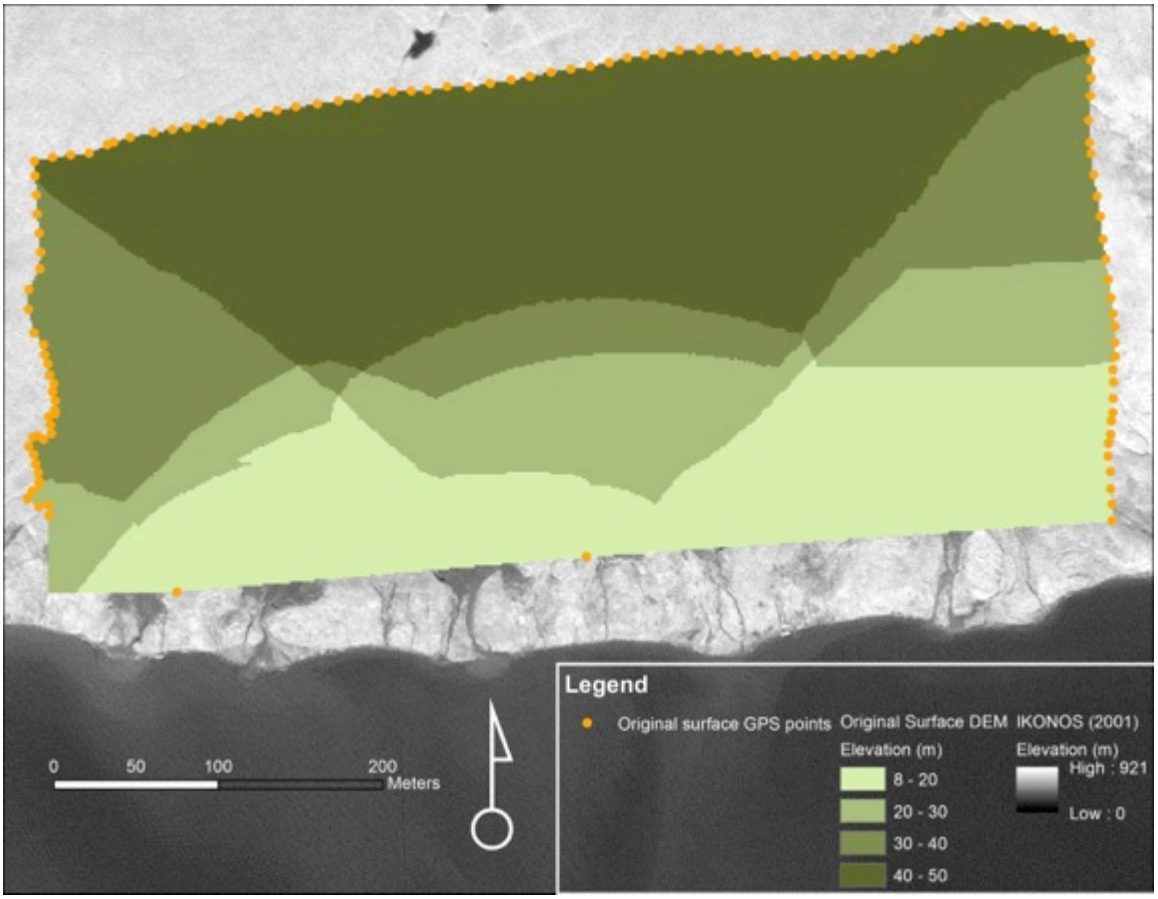


**Figure 3.4: A reconstruction of the past surface before slumping occurred. DGPS points were taken along the ridge above the three study slumps and along the coast. These points were then interpolated using the krige method.**

# CHAPTER 4 - RESULTS

## 4.1 - DGPS Slump Regression

The dGPS time series is the basis of this entire study, with the points giving an exact location and elevation of the thaw slump headwall in the summer of each year between 2004 and 2012 (Figure 4.1).

These lines challenge the current assumptions that thaw slumps regress back into the landscape between 5-10m per year (Burn & Lewkowicz, 1990). Several years show dynamic regression of almost 20m per year.

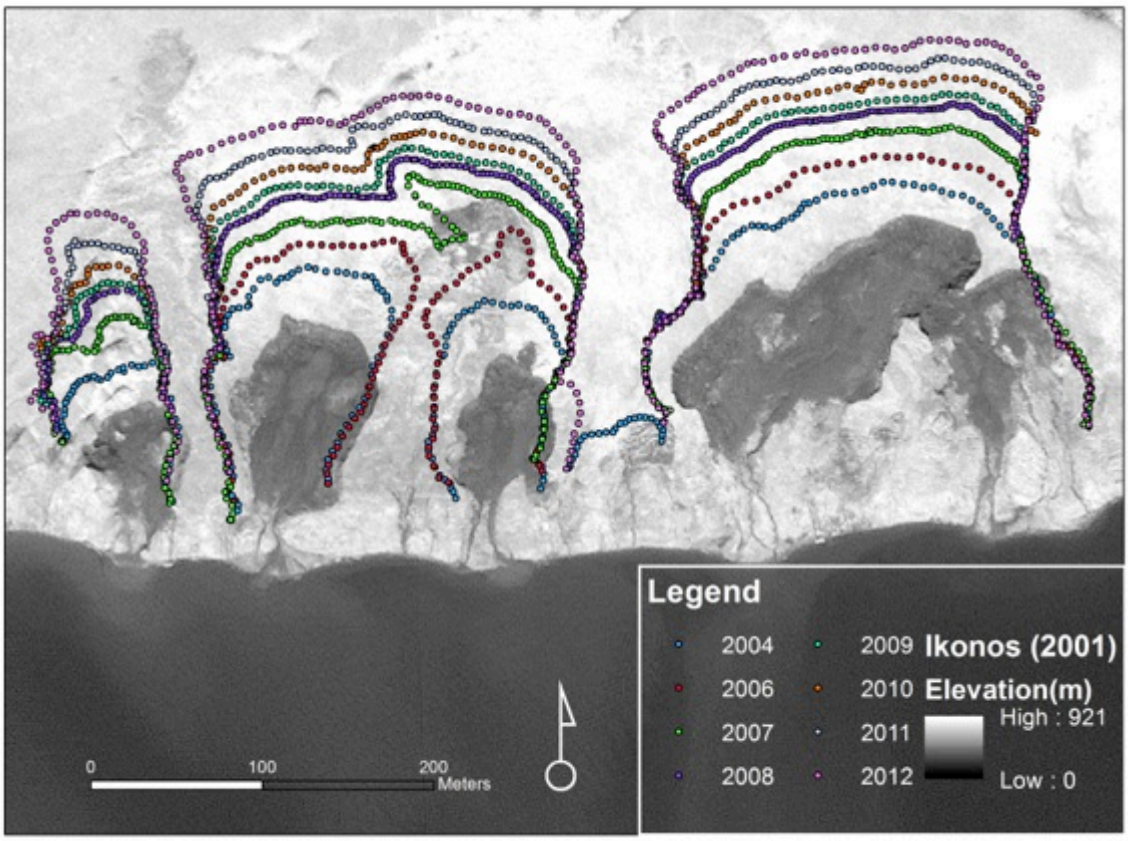


**Figure 4.1: dGPS points taken along the headwalls of slumps A, B, and C each year from 2004-2012. The points were taken at 5m intervals approximately 0.5m away from the edge, and have sub-5 cm accuracy both horizontally and vertically (Trimble, 2005).**

Table 4.1 shows the maximum retreat in metres per year for each slump. The average retreat of approximately 10m per year corresponds with previous papers, however the actual amount varies greatly between years. A high amount of retreat for slumps A (16.1m) and B (14m) can be seen between 2006 and 2007, corresponding to the high amount of erosion seen in Figure 4.2. The lowest amount of retreat for each slump occurs between 2008 and 2009.

**Table 4.1: Erosion in metres for slumps A, B, and C between 2004 and 2012. On average the slumps show an approximate 10m retreat, however this value varies widely between years.**

| Year | Slump A | Slump B | Slump C |
|---|---|---|---|
| 2004-2005 | 8.2 | 7.5 | 5.4 |
| 2005-2006 | 8.2 | 7.5 | 5.4 |
| 2006-2007 | 16.1 | 14 | 5.4 |
| 2007-2008 | 11.8 | 15 | 19.2 |
| 2008-2009 | 6.3 | 4.6 | 6.8 |
| 2009-2010 | 11.6 | 11.2 | 7.9 |
| 2010-2011 | 8.6 | 10.9 | 6 |
| 2011-2012 | 12.5 | 15.2 | 18.4 |
| **Average** | 10.4 | 10.7 | 9.3 |

## 4.2 - Individual Slump Losses

Slumps B and C have relatively similar characteristics, with an initial high amount of loss that decreases to its lowest point between 2008 and 2009, then increases until the present (Figure 4.2). Slump B encompasses a large anomaly, wherein two smaller slumps merged to form one large slump between 2006 and 2007 (Appendix B). This anomaly alone resulted in the loss of over 43,000 cubic

metres of soil. Figure 4.3 shows that a large erosion spike occurred between 2006 and 2007 in both slumps A and B, but not in C.

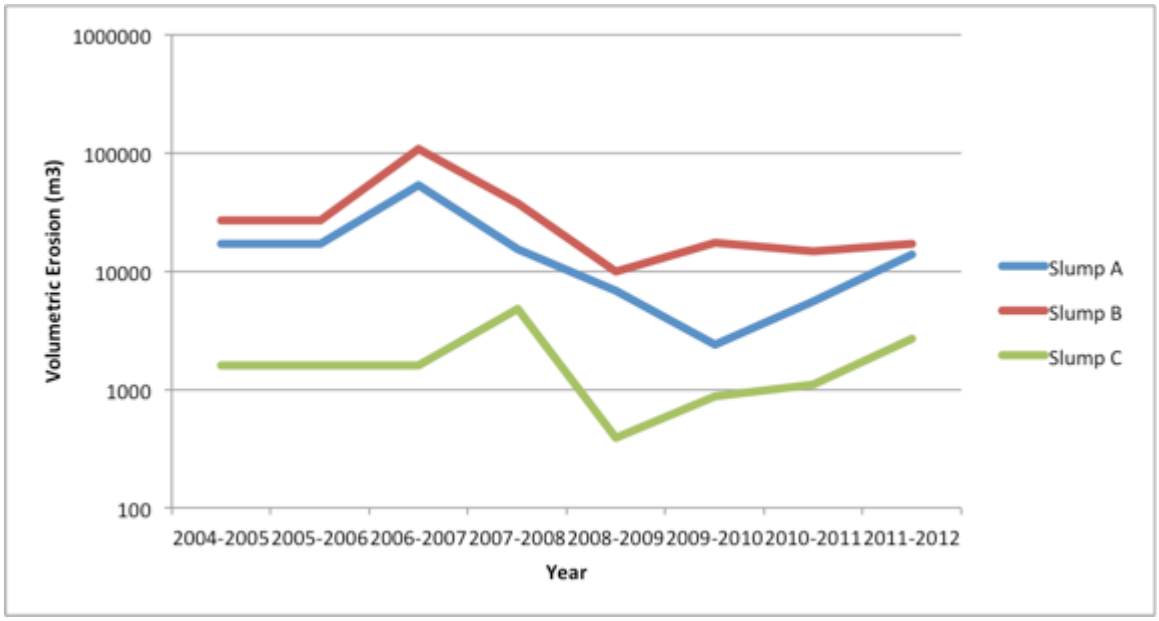


**Figure 4.2: Amount of soil erosion over time for slumps A, B, and C. A large erosion spike in slumps A and B corresponds to the year between 2006-2007.**

## 4.3 - Cumulative Sediment and SOC Loss Over Time

Cumulative sediment loss over time is shown in Figure 4.3, with a general decrease after the large anomaly between 2006 and 2007. Within all of the slumps there is a direct correlation between volume and sediment loss. A small increase in the amount of erosion can still be seen from 2008 – 2012, especially over the last three years. The lowest amount of loss was found between 2008 and 2009, while the largest amount was found between 2006 and 2007. This relatively large amount of volumetric loss is due to the data anomaly discussed above (Appendix B). A map of the slumps and their respective volumetric losses is given in Appendix B. Overall the

total amounts of both volumetric soil loss and soil organic carbon flux were substantial at over 162,000 $m^3$ and 13,400 tons respectively (Appendix C).

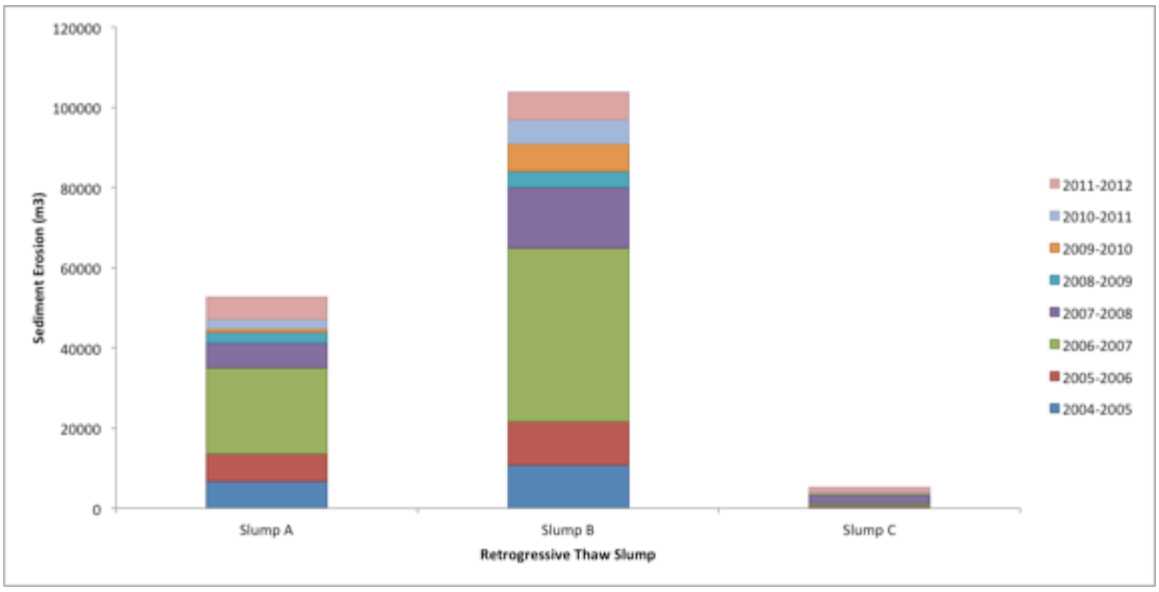


**Figure 4.3: Amount of soil erosion for each slump, showing the comparison between slumps A, B, and C. The dramatic differences between the amounts of erosion for each slump are indicative of their size differences. In total, these landforms contributed ~160,000m3.**

With 86kg of SOC in every $m^3$ of sediment, these three thaw slumps contribute a substantial amount of SOC into the Arctic Ocean each year. Figure 4.4 shows the SOC flux each year, with the maximum occurring between 2006 and 2007 when slump B alone had a SOC flux of almost 3.6 million kg.

Slump C contributed much less SOC than either slump A or B due to its size. Throughout the entire eight-year study period, slump A had an SOC flux of over 4.3 million kg, slump B of over 8.6 million kg, and slump C of over 430,000 kg. The amount of SOC flux is directly proportional to the volumetric sediment loss.

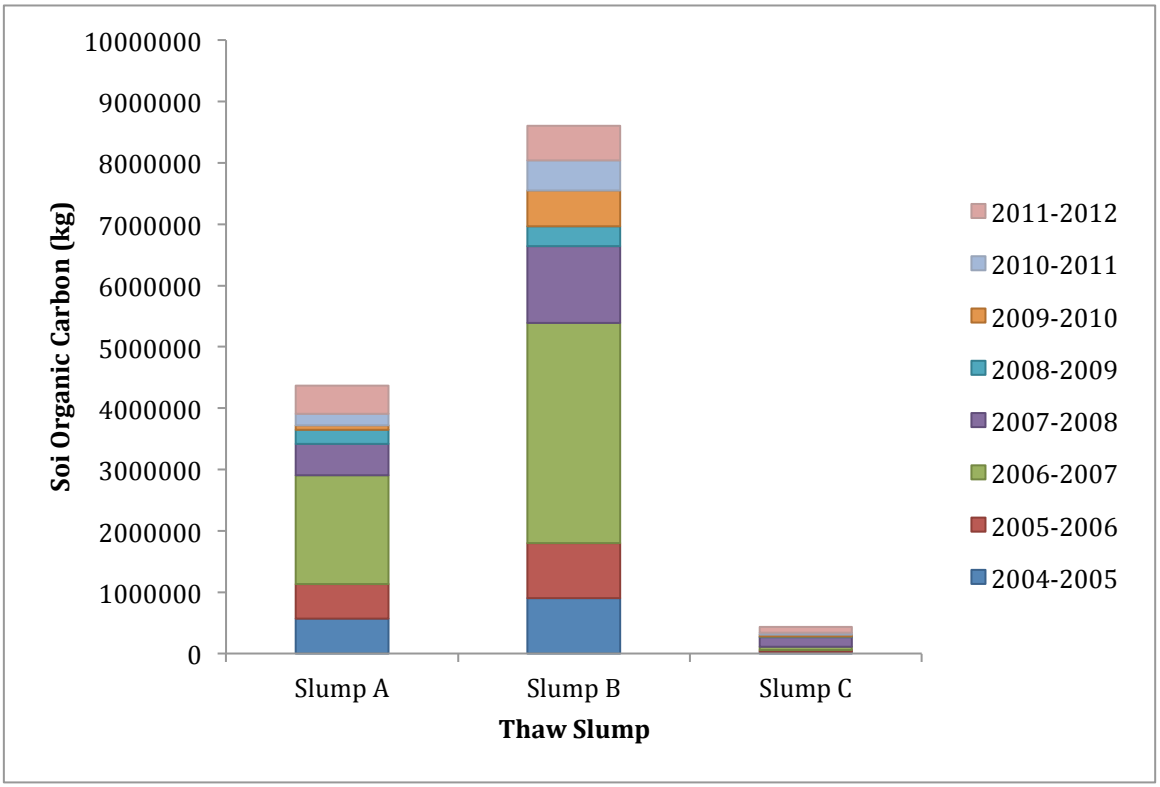


**Figure 4.4: Soil organic carbon (SOC) flux for slumps A, B, and C between 2004 and 2012. Over the eight-year study period these three slumps alone contributed an estimated 13,400 tons into the Arctic Ocean.**

## 4.4 - Percent Area Loss

The percentage of area loss for each slump was calculated to determine whether the size of the slump is a major factor in the erosion rate. In 2012, slump B was the largest at approximately 68,000m$^2$, slump A the next largest at 60,000m$^2$, and slump C the smallest at 12,000m$^2$. Figure 4.5 shows that the percent area loss is similar, with slump C (45%) having an almost identical percent area loss as slump B (50%) despite their difference in size. Slump A however experienced the least percentage of area loss (30%), even though its size is similar to that of Slump B.

The area loss for each year also varies between the slumps, the largest discrepancy in slump B between 2006 and 2007. In that year alone, slump B lost 17% of its total area. 2011 to 2012 was a dynamic year for slump C as well, with

approximately 11% of its total area being lost. The smallest loss was seen between 2008 and 2009, with each slump losing approximately 2% of its total area. All other years have approximately the same amount of loss; with slump A demonstrating slightly lower percentages (Appendix C).

When the slumps first became active is unknown, however their presence before the study commenced indicates that Slump B is growing the fastest, with over 50% of its initial area lost in the last 8 years. Slump C is slightly less with over 45% lost.

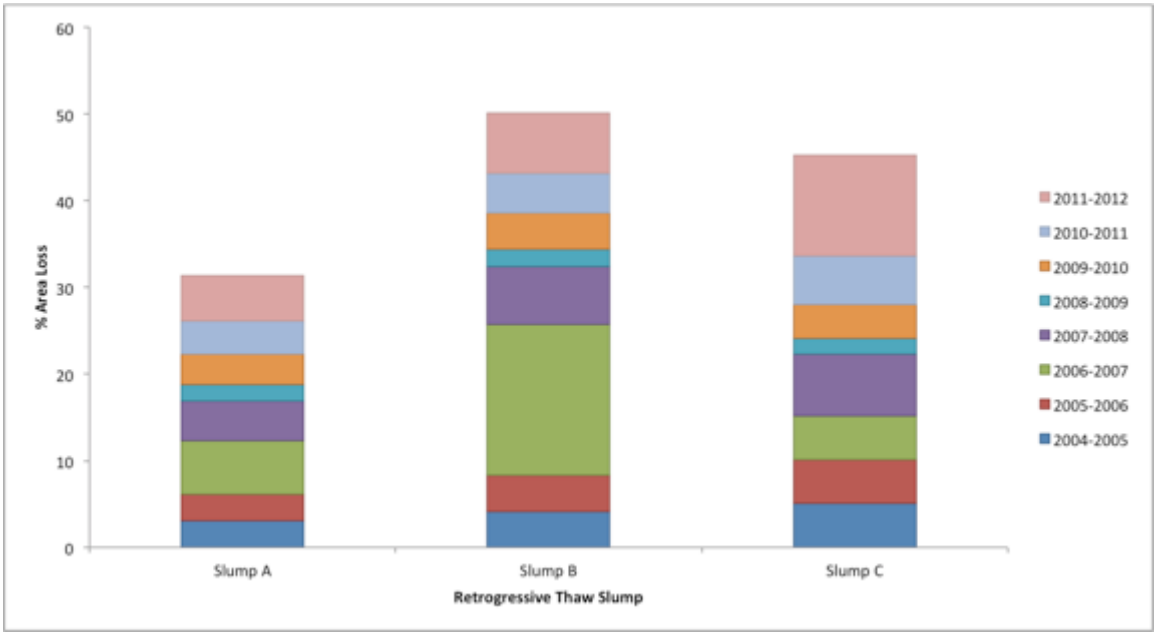


**Figure 4.5: Percent area loss for slumps A, B, and C. While slump C is the smallest in area, it has eroded a similar amount to slump B in terms of the percentage of their respective total area.**

# CHAPTER 5 - DISCUSSION

## 5.1 – DGPS Slump Regression

The DGPS time series data was integral to this study, and provided accurate positioning for the headwall outlines for each year. The points enabled a successful modeling of past landscapes, and were uniquely able to quantify the amount of volumetric erosion over the study period.

From these points it can be shown that the three slumps studied are typical in the amount of retreat they experience each year, with the headwall regressing back into the landscape an average of 10m per year (Table 4.1). The amount of retreat however, varies widely between years and slumps. Retreat rates for all three slumps range from approximately 5m between 2008 and 2009, and almost 16m between 2007 and 2008. While the average retreat over the eight-year study period is very similar for all three slumps, each has its own character. Slump C is shown to be the most dynamic, with retreat rates ranging from approximately 5m to almost 20m in two different years. Slump A and B are less dynamic, with retreat rates corresponding closer to the average. The retreat rates correspond directly with total sediment loss, giving a clear indication that slump retreat and volumetric loss are intrinsically linked. Retreat rates of almost 20m show that previous generalizations of 5-10m per year (Burn & Lewkowicz, 1990) are incorrect. Such generalizations are unscientific due to all of the different factors that affect erosional processes. A better assumption would be that retreat rates can vary from 5-20m per year depending on

the ground-ice content of the soil and the number of thaw degree days in a given year.

## 5.2 – Individual Slump Losses

These three thaw slumps are very dynamic landforms, and each has it's own character. As such, each slump should be considered both individually and in combination with the other two in order to better understand the geomorphology of the area.

Slump A is the second largest slump within this case study at 60,000$m^2$. The last three years show an approximately linear increase in the amount of regression for slump A, closely matching the similar trend found in both B and C (Figure 4.2).

Slump B is the largest of all three slumps with an area of 68,000$m^2$ and contributes a relatively massive amount of sediment flux into the Arctic Ocean each year. The amount of erosion that occurred between 2006 and 2007 is especially high at over 43,000$m^3$, when two smaller retrogressive thaw slumps merged. The year shows an obvious erosion spike in Figure 4.2; however this spike occurs in slump A as well. As the erosion spike occurs in both slump A and B, it can be assumed that the year was particularly dynamic, and that this large amount of erosion caused the two slumps within B to merge instead of the two slumps merging causing a large erosion spike.

Slump C's small size means that volumetrically it contributes little to the total amount of flux into the Arctic Ocean, but is an interesting case considering the average rate at which it retreats (~10m/yr) is the same as both slump A and B. This

fact suggests that even though C is smaller in total area (12,000m$^2$), it regresses back into the island's landmass at a similar rate as slumps A and B (much larger at 60,000m$^2$ and 68,000m$^2$ respectively). This similar rate of retreat suggests that size is not a major determinate of regression rate.

Instead, climate seems to be a large factor in determining the regression rate of thaws slumps. Figure 5.2 shows the number of thaw degree days (days with a mean temperature above 0°C) for each year. A correlation between thaw degree days and amount of retreat is evident, with the curves closely following each other. During 2006 there were 168 days above 0°C, causing the large spike in erosion between 2006 and 2007. Similar increases can be seen in 2008 (151 days) and 2012 (163 days) corresponding to similar increases in erosion for all three slumps.

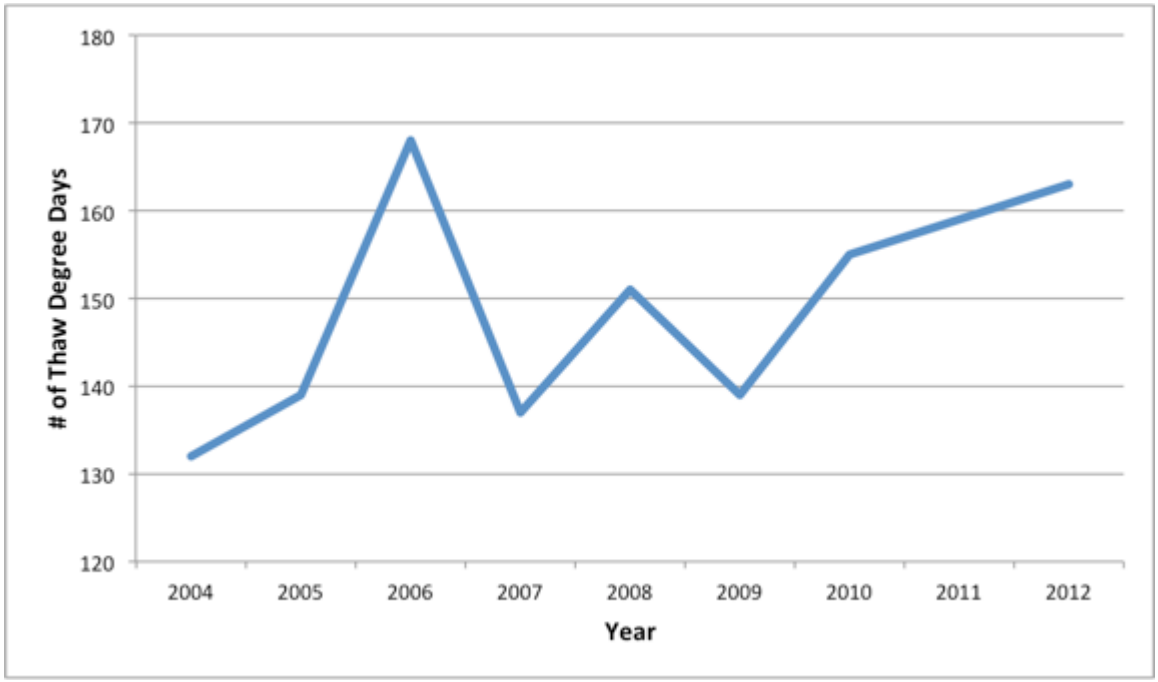


**Figure 5.2: Thaw degree days (days above 0*C) for each year in Inuvik, NWT (Environment Canada). The trend follows closely with the erosion trends shown above, with dramatic increases in the number of days in 2006, 2008, and 2012.**

## 5.3 – Cumulative Sediment and SOC Loss

Over the eight-year study period slumps A, B, and C have contributed large amounts of sediment, and everything contained within the sediment, into the Arctic Ocean. All three slumps show a positive correlation between volumetric loss, sediment loss, SOC loss, and retreat rate. This correlation could be used for later analysis to estimate the amount of contaminants and/or nutrients that are present within the sediment (e.g. mercury, soil organic carbon, etc.), and thus flow into the Arctic Ocean each year. Overall, the total amount of both volumetric and sediment loss were substantial, at over 400,000$m^3$ and 160,000$m^3$ respectively (Appendix C). The volumetric loss is considerably larger than the sediment loss due to the large amounts of cryotic material entrained within the sediment (e.g. massive ice bodies). The amount of ice within the sediment is estimated at a 60:40 ratio, with sediment contributing only 40% while excess ice contributing 60% of the entire volumetric loss (Couture, 2010).

## 5.4 – Soil Organic Carbon flux

SOC flux values were found to be much higher than anticipated based on previous studies (Lantuit & Pollard, 2005) emphasizing the importance of this case study. Slump A and B were found to input hundreds of thousands of kilograms of soil organic carbon each year, and even the smaller slump C contributed tens of thousands of kg (Appendix C). High SOC flux values are particularly worrisome, as soil organic carbon has a large impact on local and global ecosystems. High SOC levels have already degraded Arctic fisheries, negatively impacting on Inuit lifestyles

(Barber et al., 2008). Further changes within the Arctic Circle could lead to the need for significant socio-economic adaptations within these communities (Barber et al., 2008). More far ranging effects could be an increase in the melting of sea ice, and a subsequent increase in coastal erosion creating a positive feedback loop (Bockheim et al., 1999).

## 5.5 – Percent Area Loss

The percentage of area loss for each year in slump A, B, and C, was calculated to determine whether the size of a slump is a major factor in its erosion rate. The large difference in size between slump C and both slump A and B would suggest that it would have a much smaller regression rate due to the substantially less surface area for solar radiation to interact with and thaw. The data shows differently however, with Figure 4.5 showing slump C with more percentage area loss (~45%) than the larger slump A (~30%) and almost the same amount as the much larger slump B (~50%). With slump C having similar characteristics as slump B, it would seem that size is not a major factor in determining the regression rate of retrogressive thaw slumps.

Slump A also exhibits a curiously low amount of percentage area loss throughout the study period. This anomaly is most likely due to the massive erosion spike of slump B between 2006 and 2007. The massive amount of erosion in slump B between 2006 and 2007 created a large anomaly within the data, increasing its percentage area loss to a higher amount than if the merging of the two slumps had not happened.

## 5.6 – Original Surface Reconstruction

A surface detailing what Herschel Island's coastline would have looked like before the beginning of the slump activity in this area was created using DGPS points and krige interpolation methods (Figure 5.3). It represents an attempt to recreate a surface thousands of years old in order to better understand the geomorphology of the area. The attempt was successful in that a surface was interpolated which encompassed the entirety of each slump and represented the contours of the land surrounding the three thaw slumps. Further study and data collection is needed to create a truly accurate surface; however the attempt illustrates the power for DGPS and remote sensing technologies for landscape reconstruction.

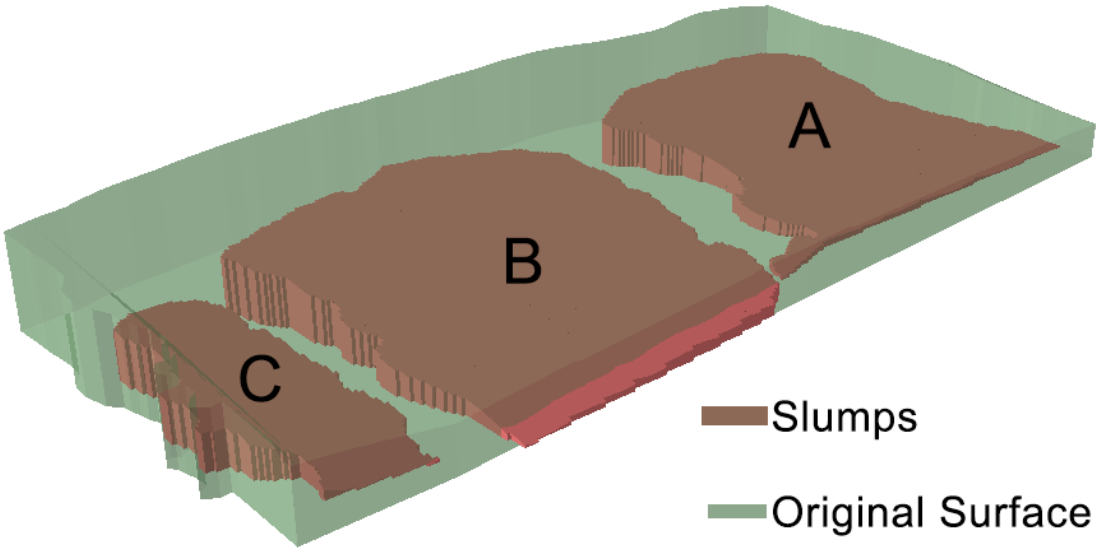


Figure 1.3: Visual representation of the surface recreation.

## 5.7 – Sources of Error

There are many sources of error within this study that need to be addressed. The first is the assumption that the soil to ice ratio is uniform throughout each slump. Soil to ice ratios can vary due to many different factors, including the

presence of absence of ground-ice features such as massive ice bodies or ice wedges. Without an accurate measure of sediment composition for past years however, it is impossible to accurately characterize the soil to ice ratio for each slump. A uniform distribution of 60% ice and 40% sediment taken from previous studies (Couture, 2010) and validated with samples taken in the 2012 field season was therefore assumed.

Although negligible, the second source of error involves the timing of data collection each year. Due to the logistical difficulties of field research in remote areas, DGPS points were not able to be collected on the same days each year. Instead, data collection occurred primarily between June and August. This difference in data collection timing between years could have increased or decreased the regression values. Due to the variable nature of Arctic research and the data being collected within a month of each other however, this error is considered to be negligible.

Discrepancies within the DGPS data collection are the cause of another error. For slumps A and B, data was collected in 2004, 2006, 2007, 2008, 2009, 2010, 2011, and 2012. During the 2006 field season however, slump C was deemed too dangerous for data collection to occur around its headwall. This data discrepancy means that the erosion for slump C was calculated with an initial erosion spanning three years (2004-2007), while slumps A and B span two years (2004-2006), with all proceeding years spanning only one year (e.g. 2009-2010). To correct for this error, these initial time spans were divided into one-year increments with an estimated linear regression rate. Due to the fact that slump C was deemed too active

to be measured safely in 2006, it is possible that it also experienced a dramatic increase in erosion between 2006 and 2007. This data discrepancy means that the values for the 2004-2005 and 2005-2006 study periods are only an estimate.

Within this study there are also methodological errors inherent in the interpolation process. Each slump floor DEM (section 3.3) was interpolated using hundreds of DGPS points at approximately 5m intervals. Given that each point has sub-5 cm accuracy, an error of approximately 3m horizontally and 0.5m vertically can be assumed.

The landscape reconstruction process was another aspect of this study with inherent errors. DGPS points were taken along the perimeter of the known ancient landscape; however there is no way to accurately recreate the inner area. Comparing the resultant surface to similar areas of coastline around the island however, it can be assumed that there were no large features (e.g. dramatic hills, deep riverine systems) that would create large errors.

## 5.8 – Future Applications

The use of GIS in conjunction with remote sensing for the quantification of erosion of retrogressive thaw slumps is just a small example of what could be accomplished with the techniques used in this study. With appropriate data, an estimation of past surfaces is possible, even surfaces thousands of years old. More recently, many different erosional processes (e.g. wave, river, or wind action) could be quantified to a high level of accuracy. This method could therefore be useful for many different geomorphological studies, as well as more practical uses. These

could include measuring the erosion rate along protected coastlines to project when a nesting colony might become endangered, measuring the rate of thaw for glaciers or ice islands, or quantifying the amount of erosion which occurs on mountains to better predict safe areas for development.

# CHAPTER 6 - CONCLUSION

This study found that retrogressive thaw slumps retreat at an average of 10m per year, corresponding with the current literature (Burn & Lewkowicz, 1990). The values for each year vary greatly however, with almost 20m of retreat happening in some years and only approximately 5m in others. This range suggests that thaw slumps are more dynamic landforms than previously thought, capable of massive amounts of erosion given the right conditions. These findings also suggest that the generalization of 5-10m per year of retreat given by Burn and Lewkowicz (1990) is incorrect. A more accurate statement would be that retreat rates vary between 5-20m per year depending on the mean annual air temperature and volume of ground-ice present in the sediment. As temperatures increase and climatic events become more extreme, retrogressive thaw slumps could become an even bigger source of sediment and SOC flux into the Arctic Ocean. Given the amount of nutrients and contaminants (e.g SOC, mercury, etc) entrained within coastal environments, as well as their status as prime locations for nesting sites and infrastructure, an increase in retrogressive thaw slump activity could have widespread detrimental effects on local and global ecosystems.

A landscape surface from the distant past was modeled in order to better understand the geomorphology of the land. This surface shows what the coastline around the three study sites would have looked like before the massive amount of slumping. It shows the contours of the land, and gives a general indication of the landscape, though many improvements could be made. This surface represents a simple recreation of a past landscape using DGPS and Remote Sensing techniques,

and similar techniques have the potential for many different applications in various areas of study.

The modeling of volumetric loss yielded a surprising amount of total volume sediment, and SOC flux. Total volumetric loss was calculated at over 400,000$m^3$ over the 8-year study period, equivalent to approximately 160 Olympic swimming pools or 52,000 average sized dump trucks. The area is known to be extremely ice-rich (Fritz et al., 2011), and thus has a high soil-ice ratio of 60:40, and a resulting total sediment loss of approximately 160,000$m^3$. This represents the first long scale study able to accurately quantify the amount of volumetric erosion and subsequent sediment and SOC flux from retrogressive thaw slumps. These volumetric totals could be used in many future studies to calculate the amount of contaminant and/or nutrient flux these landforms would contribute into the Arctic Ocean each year. One of the most interesting nutrients entrained within Herschel Island's unconsolidated coastlines is soil organic carbon (SOC). With over 13.4 million kg of SOC flowing into the Arctic Ocean from these three slumps over an eight-year period, retrogressive thaw slumps and coastal erosional processes are shown to be large contributors to the Arctic Ocean's carbon cycle. Rising concentrations of carbon within the Arctic Ocean can have various effects, including the reduction of sea ice extent creating a positive feedback and further increasing coastal erosional processes, and a destabilizing of the local and global ecosystems (Barber et al., 2008).

# Bibliography

Arp, C. D., Jones, B. M., Schmutz, J. A., Urban, F. E., & Jorgenson, M. T. (2010). Two mechanisms of aquatic and terrestrial habitat change along an Alaskan Arctic coastline. *Polar biology, 33*(12), 1629-1640.

Barber, D., Lukovich, J., Keogak, J., Baryluk, S., Fortier, L., & Henry, G. (2008). The changing climate of the Arctic. *Arctic*, 7-26.

Barnhart, K., Anderson, R., Overeem, I., Wobus, C., Clow, G., Urban, F., . . . Stanton, T. (2011). *Modeling the rate and style of Arctic coastal retreat along the Beaufort Sea, Alaska.* Paper presented at the AGU Fall Meeting Abstracts.

Bockheim, J., Everett, L., Hinkel, K., Nelson, F., & Brown, J. (1999). Soil organic carbon storage and distribution in arctic tundra, Barrow, Alaska. *Soil Science Society of America Journal, 63*(4), 934-940.

Brown, J., Jorgenson, M. T., Smith, O. P., & Lee, W. (2003). *Long-term rates of coastal erosion and carbon input, Elson Lagoon, Barrow, Alaska.* Paper presented at the Eighth International Conference on Permafrost, Balkema, Rotterdam.

Brown, R. J. E. (1960). The distribution of permafrost and its relation to air temperature in Canada and the USSR. *Arctic, 13*(3), 163-177.

Burn, C., & Lewkowicz, A. (1990). Canadian Landfrom Examples: 17 Retrogressive Thaw Slumps. *The Canadian Geographer/Le Géographe canadien, 34*(3), 273-276.

Couture, N. J. (2010). *Fluxes of Soil Organic Carbon from Eroding Permafrost Coasts, Canadian Beaufort Sea.* McGill Univeristy, Montreal, Quebec.

Forbes, D., Kremer, H., Lantuit, H., Rachold, V., & Reiersen, L. (2011). State of the Arctic Coast 2010—scientific review and outlook. International Arctic Science Committee, Land–Ocean Interactions in the Coastal Zone, Arctic Monitoring and Assessment Programme. *International Permafrost Association. Helmholtz-Zentrum, Geesthacht.*

French, H. (2007). *The periglacial environment*: Wiley.

Fritz, M., Wetterich, S., Meyer, H., Schirrmeister, L., Lantuit, H., & Pollard, W. H. (2011). Origin and characteristics of massive ground ice on Herschel Island (western Canadian Arctic) as revealed by stable water isotope and Hydrochemical signatures. *Permafrost and Periglacial Processes, 22*(1), 26-38.

Hoque, M. A., & Pollard, W. H. (2009). Arctic coastal retreat through block failure. *Canadian Geotechnical Journal, 46*(10), 1103-1115.

Johnston, G. H., ed., . (1981). *Permafrost: Engineering Design and Construction*. New York: John Wiley & Sons.

Jones, B., Arp, C., Jorgenson, M., Hinkel, K., Schmutz, J., & Flint, P. (2009). Increase in the rate and uniformity of coastline erosion in Arctic Alaska. *Geophysical Research Letters, 36*(3).

Lantuit, H., Overduin, P. P., Couture, N., Wetterich, S., Aré, F., Atkinson, D., Forbes, D. L. (2012). The Arctic Coastal Dynamics database: A new classification scheme and statistics on Arctic permafrost coastlines. *Estuaries and coasts, 35*(2), 383-400.

Lantuit, H., & Pollard, W. H. (2005). Temporal stereophotogrammetric analysis of retrogressive thaw slumps on Herschel Island, Yukon Territory. *Geomorphology, 95*(1-2), 84-102.

Mackay, J. R. (1972). The world of underground ice. *Annals of the Association of American Geographers, 62*(1), 1-22.

Mars, J., & Houseknecht, D. (2007). Quantitative remote sensing study indicates doubling of coastal erosion rate in past 50 yr along a segment of the Arctic coast of Alaska. *Geology, 35*(7), 583-586.

Oechel, W. C., Vourlitis, G. L., Hastings, S. J., & Bochkarev, S. A. (1995). Change in Arctic CO^ 2 Flux Over Two Decades: Effects of Climate Change at Barrow, Alaska. *Ecological Applications*, 846-855.

Ogorodov, S. (2008). *Effects of changing climate and sea ice extent on Pechora and Kara seas coastal dynamics.* Paper presented at the Proceedings of the 9th International Conference on Permafrost.

Opsahl, S., Benner, R., & Amon, R. M. W. (1999). Major flux of terrigenous dissolved organic matter through the Arctic Ocean. *Limnology and Oceanography, 44*, 2017-2023.

Overeem, I., Anderson, R., Wobus, C., Matell, N., Urban, F., Clow, G., & Stanton, T. (2010). *The Impact of Sea Ice Loss on Wave Dynamics and Coastal Erosion Along the Arctic Coast.* Paper presented at the AGU Fall Meeting Abstracts.

Péwé, T. L. (1966). *Permafrost and its effect on life in the north*: Oregon State University Press.

Pollard, W. (1990). *The nature and origin of ground ice in the Herschel Island area, Yukon Territory.* Paper presented at the Proceedings, Fifth Canadian Permafrost Conference, Québec.

Pollard, W., & French, H. (1980). A first approximation of the volume of ground ice, Richards Island, Pleistocene Mackenzie Delta, Northwest Territories, Canada. *Canadian Geotechnical Journal, 17*(4), 509-516.

Rachold, V., Brown, J., Solomon, S., Sollid, J.-L., eds. (2003). Reports on Polar and Marine Research, Arctic Coastal Dynamics. Report of the 3rd International Workshop, University of Oslo, 2–5 December 2002. Alfred-Wegener-Institute for Polar and Marine Research, Bremerhaven, no. 443, 127 pp.

Romanovskii, N. (1961). Erosion-thermokarst depressions on the Northern part of coastal lowlands of Yakutia and Novosibirsky islands, Merzlotnye issledovaniya, Izd. *MGU, 1*, 124-144.

Shamanova, I. I. (1971). Manifestation of erosion in permafrost on the Yamal Peninsula. Izvestiya Akad. nauk SSSR, Ser. Geograf. [News of the USSR Academy of Sciences, Geographic Series], no. 2, 92–98 (in Russian; English translation, 1971, Soviet Hydrology: Selected Papers, no. 2, 198–203).

Solomon, S. M. (2005). Spatial and temporal variability of shoreline change in the Beaufort-Mackenzie region, Northwest Territories, Canada. *Geo-Marine Letters, 25*, 127-137.

Squire, V. (2007). Of ocean waves and sea-ice revisited. *Cold Regions Science and Technology, 49*(2), 110-133.

Stein, R., & MacDonald, R. W. (2004). *The organic carbon cycle in the Arctic Ocean*: Berlin: Springer.

Toutin, T., Chénier, R., & Carbonneau, Y. (2001). *3D geometric modelling of Ikonos GEO images.* Paper presented at the Conference of the Joint ISPRS Workshop on High Resolution Mapping from Space.

Trimble Navigation Limited. (2005). *Datasheet: Trimble 5700 GPS System.* [Brochure]. Dayton, Ohio: Trimble

Tsytovich, N. A. (1973). Mechanics of soils and rocks in geomechanics. *Soil Mechanics and Foundation Engineering, 10*(4), 240-245.

Vasiliev, A., Kanevskiy, M., Cherkashov, G., & Vanshtein, B. (2005). Coastal dynamics at the Barents and Kara Sea key sites. *Geo-Marine Letters, 25*(2-3), 110-120.

# Appendix A

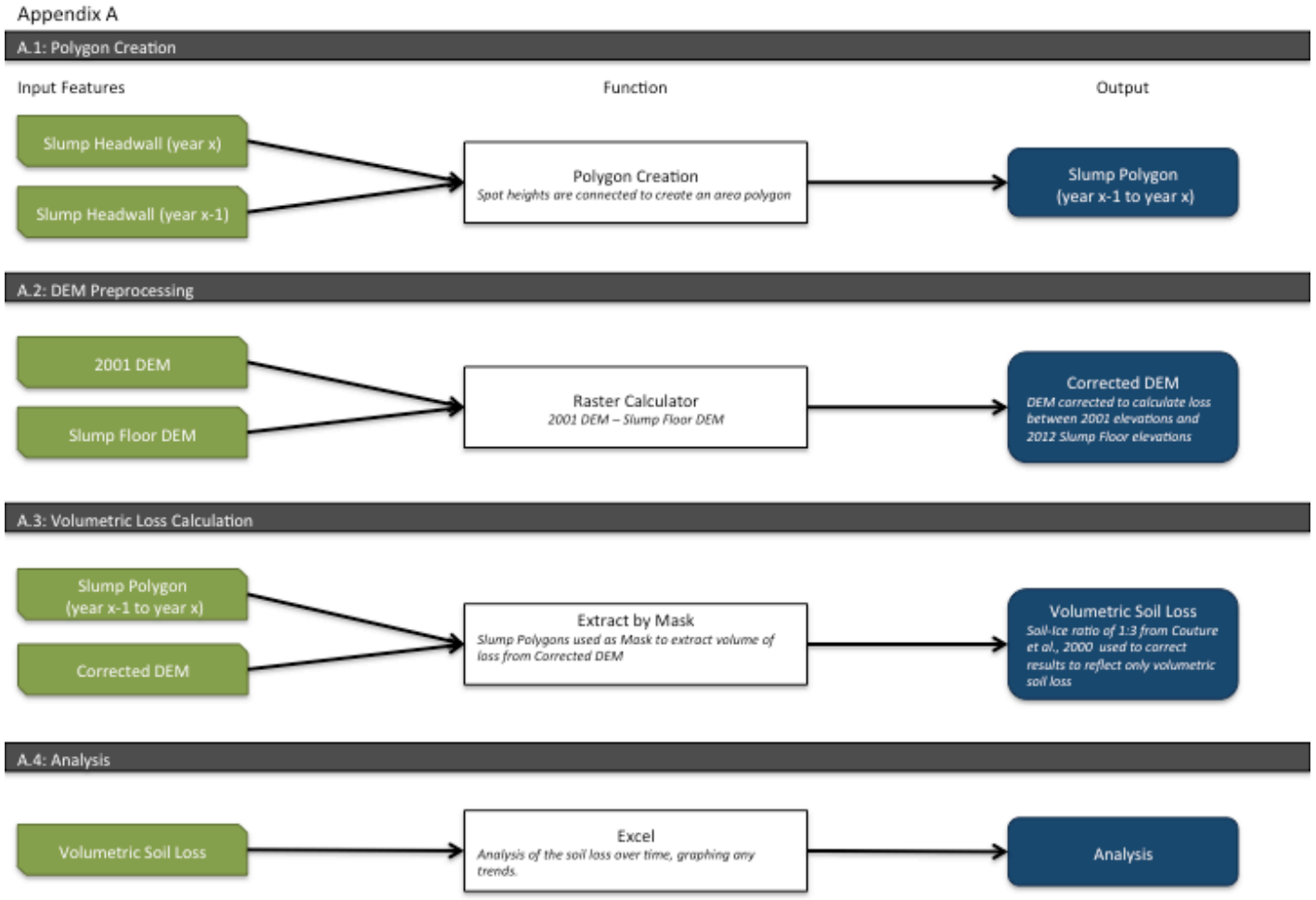
Appendix A
A.1: Polygon Creation
Input Features
Function
Output
Slump Headwall (year x)
Slump Headwall (year x-1)
Polygon Creation
Spot heights are connected to create an area polygon
Slump Polygon
(year x-1 to year x)
A.2: DEM Preprocessing
2001 DEM
Slump Floor DEM
Raster Calculator
2001 DEM – Slump Floor DEM
Corrected DEM
DEM corrected to calculate loss between 2001 elevations and 2012 Slump Floor elevations
A.3: Volumetric Loss Calculation
Slump Polygon
(year x-1 to year x)
Corrected DEM
Extract by Mask
Slump Polygons used as Mask to extract volume of loss from Corrected DEM
Volumetric Soil Loss
Soil-Ice ratio of 1:3 from Couture et al., 2000 used to correct results to reflect only volumetric soil loss
A.4: Analysis
Volumetric Soil Loss
Excel
Analysis of the soil loss over time, graphing any trends.
Analysis

## Appendix B

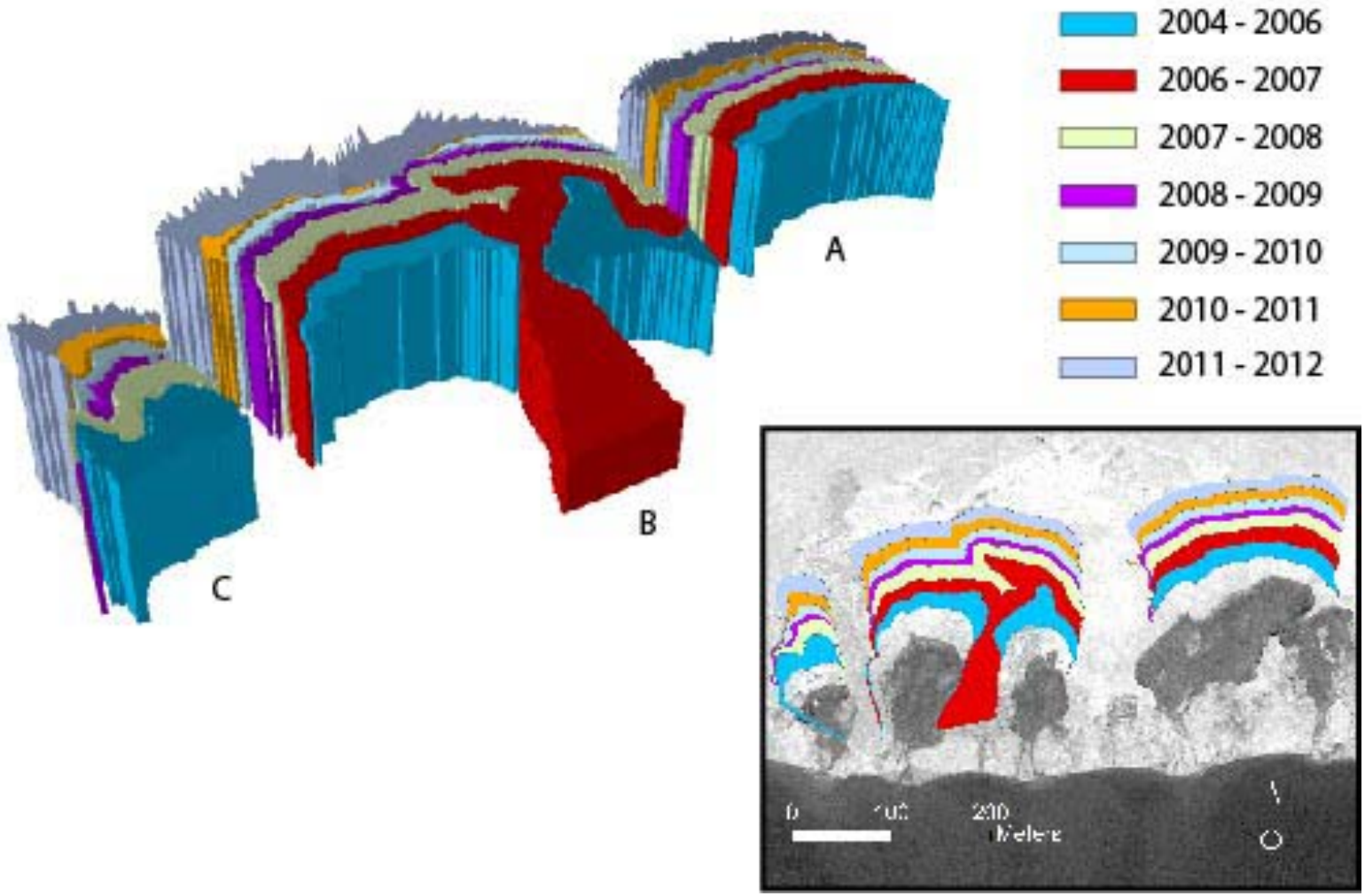
2004 - 2006
2006 - 2007
2007 - 2008
2008 - 2009
2009 - 2010
2010 - 2011
2011 - 2012
A
B
C
200
Meters

# Appendix C

| | Slump A | | |
|---|---|---|---|
| **Year** | **Volume Loss (m3)** | **Area Loss (m2)** | **SOC Flux (kg)** |
| 2004-2005 | 6820 | 1421 | 566091 |
| 2005-2006 | 6820 | 1421 | 566091 |
| 2006-2007 | 21344 | 2886 | 1771515 |
| 2007-2008 | 6182 | 2121 | 513113 |
| 2008-2009 | 2756 | 857 | 228776 |
| 2009-2010 | 959 | 1619 | 79589 |
| 2010-2011 | 2213 | 1772 | 183698 |
| 2011-2012 | 5514 | 2441 | 457649 |
| Total | 52609 | 14538 | 4366521 |
| | **Slump B** | | |
| **Year** | **Volume Loss (m3)** | **Area Loss (m2)** | **SOC Flux (kg)** |
| 2004-2005 | 10829 | 1905 | 898776 |
| 2005-2006 | 10829 | 1905 | 898776 |
| 2006-2007 | 43335 | 7959 | 3596769 |
| 2007-2008 | 15021 | 3040 | 1246723 |
| 2008-2009 | 3963 | 898 | 328893 |
| 2009-2010 | 7021 | 1906 | 582732 |
| 2010-2011 | 5934 | 2111 | 492534 |
| 2011-2012 | 6786 | 3192 | 563246 |
| Total | 103716 | 22915 | 8608450 |
| | **Slump C** | | |
| **Year** | **Volume Loss (m3)** | **Area Loss (m2)** | **SOC Flux (kg)** |
| 2004-2005 | 321 | 1603 | 26603 |
| 2005-2006 | 321 | 1603 | 26603 |
| 2006-2007 | 641 | 1603 | 53205 |
| 2007-2008 | 1909 | 4774 | 158482 |
| 2008-2009 | 155 | 388 | 12873 |
| 2009-2010 | 347 | 868 | 28807 |
| 2010-2011 | 443 | 1106 | 36731 |
| 2011-2012 | 1081 | 2702 | 89695 |
| Total | 5217 | 14645 | 432999 |